Scientific Research Publishing

World Journal of Condensed Matter Physics, 2026, 16(3), 37-54
https://www.scirp.org/journal/wjcmp
ISSN Online: 2160-6927
ISSN Print: 2160-6919

# Temperature and Composition Reliance of the Mixing Properties of Fe-Mn Melts by Molecular Interaction Volume Model

**Nabin Kumar Roy[1], Nirjar Vrind[2], Sunil Kumar Bhagat[2], Ranjan Prabhu[2], Jagdhar Mandal[2*], Indu Shekhar Jha[3]**

[1]University Department of Chemistry, T.M. Bhagalpur University, Bhagalpur, India
[2]University Department of Physics, T.M. Bhagalpur University, Bhagalpur, India
[3]Department of Physics, M.M.A.M. Campus, Biratnagar, Nepal

Email: nabinkrroy@gmail.com, nirjarvrind9931@gmail.com, bhagatsunilkumar0013@gmail.com, b84083777@gmail.com, *jmandal1284@gmail.com, isjha12345@gmail.com

**How to cite this paper:** Roy, N.K., Vrind, N., Bhagat, S.K., Prabhu, R., Mandal, J. and Jha, I.S. (2026) Temperature and Composition Reliance of the Mixing Properties of Fe-Mn Melts by Molecular Interaction Volume Model. *World Journal of Condensed Matter Physics*, **16**, 37-54.
https://doi.org/10.4236/wjcmp.2026.163003

**Received:** June 26, 2026
**Accepted:** August 28, 2026
**Published:** August 31, 2026



## Abstract

The mixing properties of Fe-Mn melts have been explored as a function of composition of Fe at 1763 K, 1863 K, 1963 K and 2063 K on utilizing molecular interaction volume model. The analytical expressions for the thermodynamic variables like excess free energy of mixing, Gibbs free energy of mixing, activity and activity coefficients of a binary alloy are deduced and these expressions are employed to ascertain the theoretical data of the thermodynamic functions for Fe-Mn melts at the temperatures under consideration. For this, the required interaction energy parameters are estimated by Newton-Rapson method on employing the experimental value of activity coefficient at infinite dilution. The theoretical values of the thermodynamic properties are compared with the correlated experimental data available in the literature for Fe-Mn melts at 1863 K. An excellent harmony is observed. Again, the expression for the microscopic function like concentration fluctuations for a binary system is deduced in the framework of molecular interaction volume model. The theoretical data of the concentration fluctuations for Fe-Mn melts are reckoned at 1763 K, 1863 K, 1963 K and 2063 K. The theoretical and experimental data of concentration fluctuations exhibit well harmony at 1863 K. Further, the analytical expressions for short-range order parameter, diffusivity ratio and excess stability function for a binary system are also derived in terms of concentration fluctuations. The analytical expressions are employed to theoretically predict the short-range order parameter, diffusivity ratio and excess stability function of

Fe-Mn melts at 1763 K, 1863 K, 1963 K and 2063 K. The results predict the feebly segregating character of Fe-Mn melts in the temperature range 1763 - 2063 K.

## Keywords

Molecular Interaction Volume Model, Gibss Free Energy of Mixing, Activity Coefficient, Concentration Fluctuations, Excess Stability Function and Diffusivity Ratio

## 1. Introduction

The iron-manganese (Fe-Mn) and Fe-Mn-based alloys have a wide range of applications in steel productions, welding industries, as catalysts and medicines, in paints, etc. For high-strength constructional materials, there are extensive applications of Fe-Mn system. The element Mn is an important alloy constituent associated with a number of ferroalloys and steels, *i.e.* twining induced plasticity and transformation induced plasticity steels, in order to make the material hard [1] [2]. The phase diagram [3] illustrates that Fe-Mn is a symmetric alloy in terms of $G_M^E$ and $G_M$. Again, the positive values of $G_M^E$ at each composition of Fe and the positive deviations of the activities of Fe and Mn from linearity signify the segregating character of Fe-Mn melts at 1863 K. Thus, Fe-Mn melts have drawn the attentiveness of several investigators [1] [2] [4]-[13] to explain the thermophysical behavior of Fe-Mn melts. However, the theoretical exploration of the alloying behaviour of Fe-Mn melts is scarce in the literature. Recently, Ogundeji *et al.* have applied self-association model [13] to explain the free energy of mixing, $G_M$, activity of Fe, concentration fluctuations, $S_{cc}(0)$, Warren-Cowley [14] [15] short-range order parameter, $\alpha_1$, diffusivity, D and viscosity of Fe-Mn melts at 1863 K. Nevertheless, the theoretical explanation of the thermodynamic functions like excess free energy of mixing, $G_M^E$, activity of Mn, activity coefficient, $\gamma_{Fe}$ and $\gamma_{Mn}$ as well as excess stability function, $E^{XS}$ for Fe-Mn melts are not reported in the literature. Therefore, the thermophysical properties of Fe-Mn melts require further theoretical analysis.

The aim of the present work is to explore the thermodynamic, structural and transport functions of Fe-Mn melts at 1863 K by MIVM (*i.e.* molecular interaction volume model) presented by Tao [16]. Earlier MIVM model has been successfully utilized to analyse the thermodynamic functions of various binary melts such as Zn-Bi, Au-Ni, Au-Cu, Au-Pd, Ti-Al, Zn-Cd etc. [17]-[20] and ternary melts such as In-Bi-Sn, Al-Sn-Zn, Sn-Ag-Cu, Zn-Cu-Sn-In [21]-[24]. Therefore, MIVM model has been employed to predict the concentration dependence of the thermophsical properties like $G_M^E$, $G_M$, $a_{Fe}$, $a_{Mn}$, $\gamma_{Fe}$, $\gamma_{Mn}$, $S_{cc}(0)$, $\alpha_1$, $E^{XS}$ and $D_M/D_{id}$ of Fe-Mn melts at 1763 K, 1863 K, 1963 K and 2063 K.

## 2. Formalism

### 2.1. Thermodynamic Properties *i.e.* Excess Free Energy of Mixing, $G_M^E$, Free Energy of Mixing, $G_M$, Activity Coefficient, $\gamma_\mu$ and Activity, $a_\mu(\mu = i, j)$ of Binary Molten Alloys

The fluid based model MIVM has been introduced by Tao [16] and deduced from statistical thermodynamics, fluid-phase equilibria and the fundamental concept of the non-random exchange of liquid molecules. The molecular excess free energy of mixing of a binary molten alloy *i-j* is expressed as [16]

$$\frac{G_M^E}{RT} = x_i \ln\left(\frac{V_{mi}}{x_i V_{mi} + x_j V_{mj} A_{ji}}\right) + x_j \ln\left(\frac{V_{mj}}{x_j V_{mj} + x_i V_{mi} A_{ij}}\right) - \frac{x_i x_j}{2}\left(\frac{Z_i A_{ji} \ln A_{ji}}{x_i + x_j A_{ji}} + \frac{Z_j A_{ij} \ln A_{ij}}{x_j + x_i A_{ij}}\right) \tag{1}$$

where, $x_i$ and $x_j$ are the compositions (or mole fractions) of *i* and *j* components respectively; $Z_i$ and $Z_j$ represent the first coordination numbers for *i* and *j* molecules respectively. $A_{ij}$ and $A_{ji}$ refer to pair-potential energy interaction parameters, expressed as [16]

$$A_{ji} = \exp\left[-\frac{\varepsilon_{ji} - \varepsilon_{ii}}{kT}\right] \text{ and } A_{ij} = \exp\left[-\frac{\varepsilon_{ij} - \varepsilon_{jj}}{kT}\right] \tag{2}$$

where, $\varepsilon_{ii}$, $\varepsilon_{jj}$ and $\varepsilon_{ji}$ = pair potential energies for *i-i*, *j-j* and *i-j* respectively, in which $\varepsilon_{ji} = \varepsilon_{ij}$, $k$ = Boltzmann constant and $T$ = temperature in K of the liquid metal.

The partial molar free energy and molar excess free energy are related to

$$G_M^{\tilde{E}} = RT \ln \gamma_i = G_M^E + \delta\left(\frac{\partial G_M^E}{\partial x_i}\right)_{T,P,x[i,N]} - \sum_{j=1}^{N}\left(\frac{\partial G_M^E}{\partial x_i}\right)_{T,P,x[j,N]} \tag{3}$$

It is necessary to mention that the above equation is based on the condition such that when $i \neq N$, $\delta = 1$; and $i = N$, $\delta = 0$. Again, $x[i,N]$ defines the variables $x_j$ and $x_N$ where, $x_N = 1 - \sum_{j=1}^{N-1} x_j$. Therefore, the activity coefficients of $i$ and $j$ elements of a binary alloy are, respectively, expressed as

$$\ln \gamma_i = \ln\left(\frac{V_{mi}}{x_i V_{mi} + x_j V_{mj} A_{ji}}\right) + x_j\left(\frac{V_{mj} A_{ji}}{x_i V_{mi} + x_j V_{mj} A_{ji}} - \frac{V_{mi} A_{ji}}{x_j V_{mj} + x_i V_{mi} A_{ij}}\right) - \frac{x_j^2}{2}\left(\frac{Z_i A_{ji}^2 \ln A_{ji}}{\left(x_i + x_j A_{ji}\right)^2} + \frac{Z_j A_{ij} \ln A_{ji}}{\left(x_j + x_i A_{ij}\right)^2}\right) \tag{4}$$

and

$$\ln \gamma_j = \ln\left(\frac{V_{mj}}{x_j V_{mj} + x_i V_{mi} A_{ij}}\right) - x_i\left(\frac{V_{mj} A_{ji}}{x_i V_{mi} + x_j V_{mj} A_{ji}} - \frac{V_{mi} A_{ij}}{x_j V_{mj} + x_i V_{mi} A_{ij}}\right) - \frac{x_i^2}{2}\left(\frac{Z_j A_{ij}^2 \ln A_{ij}}{\left(x_j + x_i A_{ij}\right)^2} + \frac{Z_i A_{ji} \ln A_{ji}}{\left(x_i + x_j A_{ji}\right)^2}\right) \tag{5}$$

Now, the first co-ordination number of $i^{th}$ component can be achieved on using the relation [16]

$$Z_i = \frac{4\sqrt{2\pi}}{3}\left(\frac{r_{mi}^3 - r_{oi}^3}{r_{mi} - r_{oi}}\right)\rho_i r_{mi} \exp\left(\frac{\Delta H_{mi}\left(T_{mi} - T\right)}{Z_C R T_{mi}}\right) \tag{6}$$

with $\Delta H_{mi}$ is the enthalpy at melting temperature, $T_{mi}$ and $Z_C$ is taken to be 12 for closed packed structure; $\rho_i = N_i V_i = \frac{0.6022}{V_{mi}}$ molecular number density; $r_{mi}$ and $r_{oi}$ = initial and first peak values of radial distribution function for the molten metal $i$ near melting temperature, respectively, and $R$ is the molar gas constant. The radial distances are expressed as

$$r_{oi} = 0.918 d_{covi} \quad \text{and} \quad r_{mi} = \sigma_i \tag{7}$$

where, $\sigma_i$ and $d_{covi}$ = atomic diameter and atomic covalent diameter respectively.

The equations for activity coefficients of the components of the alloy in infinite dilute solution range *i.e.* $x_i$ or $x_j \to 0$, are respectively given by

$$\ln \gamma_i^{\infty} = 1 - \ln\left(\frac{V_{mj} A_{ji}}{V_{mi}}\right) - \frac{V_{mi} A_{ji}}{V_{mj}} - \frac{1}{2}\left(Z_i \ln A_{ji} + Z_j A_{ij} \ln A_{ij}\right) \tag{8}$$

and

$$\ln \gamma_j^{\infty} = 1 - \ln\left(\frac{V_{mi} A_{ij}}{V_{mj}}\right) - \frac{V_{mj} A_{ji}}{V_{mi}} - \frac{1}{2}\left(Z_j \ln A_{ij} + Z_i A_{ji} \ln A_{ji}\right) \tag{9}$$

Again, the expressions for the activity of the constituents $i$ and $j$ in terms of activity coefficients are, respectively given by [25]

$$a_i = \gamma_i x_i \tag{10a}$$

$$a_j = \gamma_j x_j \tag{10b}$$

## 2.2. Microscopic Properties *i.e.* Concentration Fluctuations, $S_{cc}(0)$ and Short-Range Order Parameter, $\alpha_1$ of a Binary Molten Alloy

The concentration fluctuations, $S_{cc}(0)$ and SRO, $\alpha_1$ play a vital role to explore the interatomic interactions in a liquid melt. If $S_{cc}(0) < S_{cc}^{id}(0)$, then the alloy is ordering and dissimilar atoms or molecules (*i.e. i-j*) associate together as the closest neighbours while $S_{cc}(0) > S_{cc}^{id}(0)$ represents the segregating nature of the system *i.e.* similar atoms or molecules (*i.e. i-i* or *j-j*) associate together as the closest neighbours [25].

$S_{cc}(0)$ may be represented in terms of $G_M$ by [25] [26]

$$S_{cc}(0) = RT\left(\frac{\partial^2 G_M}{\partial x_i^2}\right)_{T,P,N}^{-1} = RT\left(\frac{\partial^2 G_M}{\partial x_j^2}\right)_{T,P,N}^{-1} \tag{11}$$

where,

$$G_M = G_M^E + G_M^{id} \tag{12}$$

$$\Rightarrow G_M = G_M^E + RT\left[x_i \ln x_i + x_j \ln x_j\right] \tag{13}$$

Equations (1), (11) and (13) yield

$$S_{cc}(0) = \frac{x_i x_j}{1 + x_i x_j f\left(x_i x_j\right)} \tag{14}$$

where,

$$\begin{aligned} f\left(x_i, x_j\right) = & \frac{V_{mj}A_{ji} - V_{mi}}{x_i V_{mi} + x_j V_{mj} A_{ji}} + \frac{V_{mi}A_{ij} - V_{mj}}{x_j V_{mj} + x_i V_{mi} A_{ij}} + \frac{V_{mj}A_{ji}\left(V_{mj}A_{ji} - V_{mi}\right)}{\left(x_i V_{mi} + x_j V_{mj} A_{ji}\right)^2} \\ & + \frac{V_{mi}A_{ij}\left(V_{mi}A_{ij} - V_{mj}\right)}{\left(x_j V_{mj} + x_i V_{mi} A_{ij}\right)^2} + \left[\frac{Z_i A_{ji}^2 \ln A_{ji}}{\left(x_i + x_j A_{ji}\right)^3} + \frac{Z_j A_{ij}^2 \ln A_{ij}}{\left(x_j + x_i A_{ij}\right)^3}\right] \end{aligned} \tag{15}$$

For the ideal mixing condition, $G_M^E = 0$, hence Equation (12) reduces to $G_M = G_M^{id}$. Therefore, Equations (14) and (15) provide

$$S_{cc}^{id}(0) = x_i x_j \tag{16}$$

which represents the ideal $S_{cc}(0)$.

Again, concentration fluctuations in terms of activity can be expressed as [25]-[27]

$$S_{cc}(0) = a_i x_j \left(\frac{\partial a_i}{\partial x_i}\right)^{-1} = a_j x_i \left(\frac{\partial a_j}{\partial x_j}\right)^{-1} \tag{17}$$

The value of $S_{cc}(0)$ computed from above equation on employing the experimental values of activity is considered as the experimental value of $S_{cc}(0)$ [25]-[27].

The SRO, $\alpha_1$ introduced by Warren-Cowley [14] [15] in terms of $S_{cc}(0)$ is represented as [25] [28]

$$\alpha_1 = \frac{S-1}{S(Z-1)+1} \quad \text{with} \quad S = \frac{S_{cc}(0)}{S_{cc}^{id}(0)} \tag{18}$$

where, $Z$ is the coordination number in first neighbor shell.

It is obvious from Equation (18) that $\alpha_1$ = positive for segregating alloys, $\alpha_1$ = negative for ordered alloys and $\alpha_1 = 0$ for ideal mixture.

### 2.3. Excess Stability Function, $E^{XS}$ and Diffusivity, $D$ of a Binary Molten Alloy

The excess stability function, $E^{XS}$ described by Darken [29] [30] can be expressed as

$$\frac{E^{XS}}{RT} = \left(S_{cc}(0)\right)^{-1} - \left(S_{cc}^{id}(0)\right)^{-1} \tag{19}$$

It is necessary to mention that $E^{XS}$ = positive for ordering alloy, $E^{XS}$ = negative for segregating alloy and $E^{XS}=0$ for ideal alloy depending upon the facts that $S_{cc}(0)<S_{cc}^{id}(0)$, $S_{cc}(0)>S_{cc}^{id}(0)$, and $S_{cc}(0)=S_{cc}^{id}(0)$ respectively.

The transport property such as diffusivity is very useful to analyse the mixing behaviour of a binary solution at the microscopic level. For a binary liquid system, the diffusivity ratio is expressed as [25] [31].

$$\frac{D_M}{D_{id}}=\frac{S_{cc}^{id}(0)}{S_{cc}(0)} \tag{20}$$

where, $D_M$ and $D_{id}$ represent mutual diffusion coefficient of the system and intrinsic diffusion coefficient for ideal system respectively. Now, $D_{id}$ is given by

$$D_{id}=x_iD_j+x_jD_i \tag{21}$$

where, $D_i$ and $D_j$ = self-diffusion coefficients of pure elements *i* and *j* respectively.

Equation (20) illustrates that $D_M/D_{id}>1$ for ordered system, $D_M/D_{id}<1$ for segregating system and $D_M/D_{id}=1$ for ideal alloy.

## 3. Results and Discussions

### 3.1. Excess Free Energy of Mixing, $G_M^E$, Free Energy of Mixing, $G_M$, Activity Coefficient, $\gamma_\mu$, and Activity, $a_\mu(\mu=i,j)$ of Fe-Mn Melts at 1863 K

The analytical equations for $G_M^E$, $G_M$, $\gamma_\mu$ and $a_\mu(\mu=i,j)$ are utilized to determine the thermodynamic properties of Fe-Mn melts at 1863 K. The necessary parameters for pure Fe and Mn are presented in **Table 1** [32]. The coordination number $Z_i$ and $Z_j$ of the constituents of alloy are determined from Equation (6) which are presented in **Table 2**. The parameter $A_{ji}$ and $A_{ij}$ are evaluated on solving Equations (8) and (9) simultaneously by Newton-Raphson method. For this, $\gamma_i^\infty$ and $\gamma_j^\infty$ *i.e.* infinite dilute activity coefficients at 1863 K are required which have been presented in **Table 2** [3]. The evaluated values of $A_{ji}$ and $A_{ij}$ are 0.9488 and 0.9410, respectively. In order to acquire good agreement between the theory and experiment [3] of Fe-Mn melts at 1863 K, the values of $A_{ji}$ and $A_{ij}$ are slightly altered. The best fit values of $A_{ji}$ and $A_{ij}$ are 0.9616 and 0.9863 respectively (included in **Table 2**). Obviously, values of $A_{ji}$ and $A_{ij}$ are increased through 1.34% and 4.8% respectively.

**Table 1.** Input parameters for the pure metals [32].

| Metal, *i* | $\Delta H_{mi}$ (KJ/mol) | $\sigma_i$ (×10$^{-8}$ cm) | $r_{oi}$ (×10$^{-8}$ cm) | $V_{mi}$ (cm$^3$/mol) |
|---|---|---|---|---|
| Fe | 13.77 | 2.56 | 1.98 | 7.94 [1 + 1.3 × 10$^{-4}$ ($T$ − 1808)] |
| Mn | 14.6 | 2.61 | 2.15 | 9.54 [1 + 1.6 × 10$^{-4}$ ($T$ − 1517)] |

**Table 2.** Estimated values of $A_{ij}$, $A_{ji}$, $Z_i$ and $Z_j$ for the constituents of Fe-Mn molten alloys at various temperatures.

| *i-j* | $T$(K) | $A_{ij}$ | $A_{ji}$ | $Z_i$ | $Z_j$ | $\gamma_i^{\infty}$ | $\gamma_j^{\infty}$ |
|---|---|---|---|---|---|---|---|
| Fe-Mn | 1763 | 0.9855 | 0.9595 | 10.15 | 9.25 | – | – |
| | 1863 | 0.9863 | 0.9616 | 10.08 | 8.89 | 1.330 | 1.330 |
| | 1963 | 0.9870 | 0.9635 | 9.89 | 8.76 | – | – |
| | 2063 | 0.9876 | 0.9653 | 9.76 | 8.63 | – | – |

Work flow of Newton-Raphson Method for calculation of $A_{ij}$ and $A_{ji}$

START → Input experimental data: T, $x_i$, $x_j$, $\gamma_i$ (exp.), $\gamma_j$ (exp.), molar volumes ($V_{mi}$ & $V_{mj}$), coordination number ($Z_i$ & $Z_j$) → Give initial guesses for $A_{ij}$ and $A_{ji}$ → Calculate $\gamma_i$ (calc.) and $\gamma_j$ (calc.) using the MIVM → Calculate residual functions: F' = $\gamma_i$ (calc.) − $\gamma_i$ (exp) & F'' = $\gamma_j$ (calc.) − $\gamma_j$ (exp) → Compute the Jacobian matrix (partial derivatives of F' and F'' with respect to $A_{ij}$ and $A_{ji}$) → Solve the Newton-Raphson equation: J ΔA = −F → Update parameters: $A_{ij}$ (new) = $A_{ij}$ (old) + $\Delta A_{ij}$ & $A_{ji}$ (new) = $A_{ji}$ (old) + $\Delta A_{ji}$ → Convergence test: $|F'| < \varepsilon$ and $|F''| < \varepsilon$ → Result is No or Yes → If No then Repeat Iteration, If Yes *i.e.* Output final values of $A_{ij}$ and $A_{ji}$

The values of $G_M^E/RT$ calculated from Equation (1) as function of Fe for Fe-Mn alloys at 1863 K exhibit excellent uniformity with the corresponding experimental values [3] as shown in **Figure 1**. In composition range, $x_{Fe} = 0.1$ to 0.9, the value of $G_M^E$ is positive at each concentration. The theoretical and experimental [3] data of $G_M^E/RT$ are in excellent harmony with maximum values at $x_{Fe} = 0.50$ *i.e.* 0.0710 (Theory) and 0.0711 (Experiment). The RMS error for $G_M^E$ is found to be 0.0000894% from Equation (22). Hence, the present theoretical investigation successfully represents the symmetry in $G_M^E/RT$ and segregating character of Fe-Mn melts at 1863 K.

$$\text{RMS Error} = \sqrt{\frac{\sum_{i=1}^{n}\left(x_i - y_i\right)^2}{n}} \tag{22}$$

where,

$x_i$ = theoretical (calculated) values;

$y_i$ = experimental values;

$n$ = no. of data points.

Equation (13) is utilized to compute the values of $G_M/RT$ for Fe-Mn melts at 1863 K, which are illustrated in **Figure 2** along with correlated experimental data [3]. A well agreement is observed. In the entire composition region, $x_{Fe} = 0.1$ to 0.9, $G_M/RT$ is negative with minimum values at $x_{Fe} = 0.5$ *i.e.* $G_M/RT\left(\min^{m}\right) = -0.6221$ (Theory) and −0.6221 (Experiment). The RMS error for $G_M/RT$ is found to be 0.00064238%. Therefore, the symmetry in $G_M/RT$ is successfully described by MIVM Model. It is notable that the minimum value of $G_M/RT$ for Fe-Mn melts at 1863 K computed by self-association model [13] is −0.615 at $x_{Fe} = 0.5$. Thus, the present theoretical model provides more accurate result in comparison to that obtained by self-association model [13].

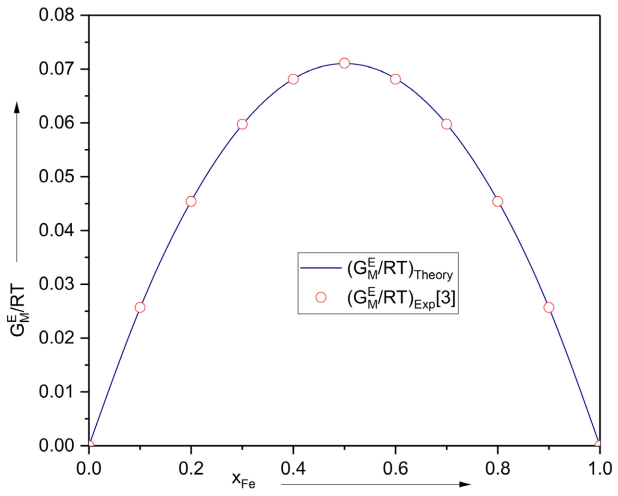


**Figure 1.** $G_M^E/RT$ vs $x_{Fe}$ for Fe-Mn melts at 1863 K.

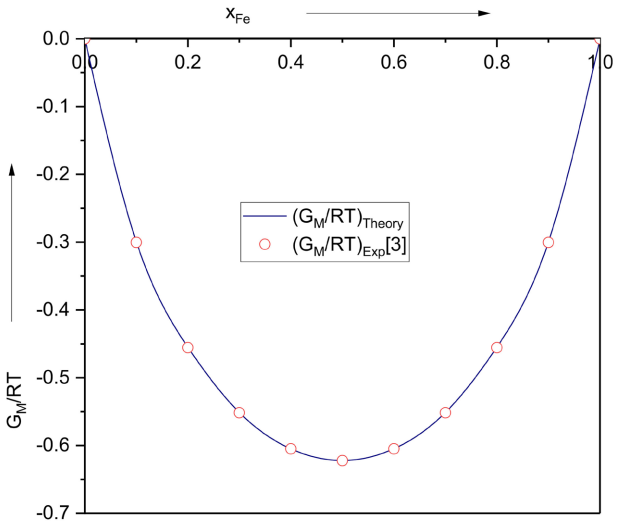


**Figure 2.** $G_M/RT$ vs $x_{Fe}$ for Fe-Mn melts at 1863 K.

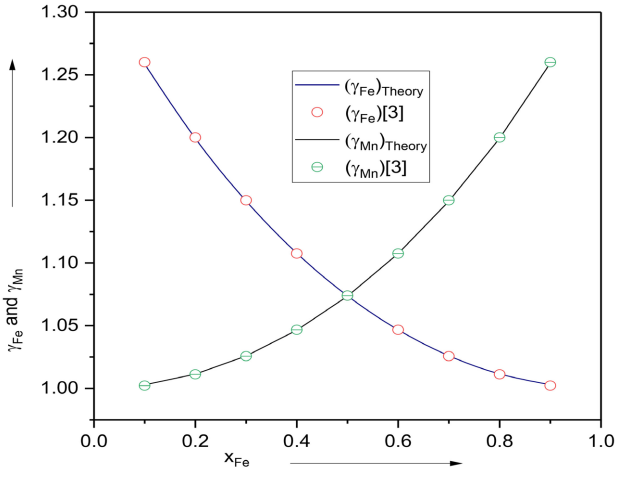


**Figure 3.** ( $\gamma_{Fe}$ & $\gamma_{Mn}$ ) vs $x_{Fe}$ for Fe-Mn melts at 1863 K.

The activity coefficients $\gamma_{Fe}$ and $\gamma_{Mn}$ are determined from Equations (4) and (5) respectively in terms of concentration for Fe. The theoretical and experimental [3] data of $\gamma_{Fe}$ and $\gamma_{Mn}$ are in excellent agreement as shown in **Figure 3**.

The theoretical data of $\gamma_{Fe}$ and $\gamma_{Mn}$ are employed to calculate the concentration dependence of $a_{Fe}$ and $a_{Mn}$ respectively from equations (10a) and (10b) for Fe-Mn melts at 1863 K, which are presented in **Figure 4**.

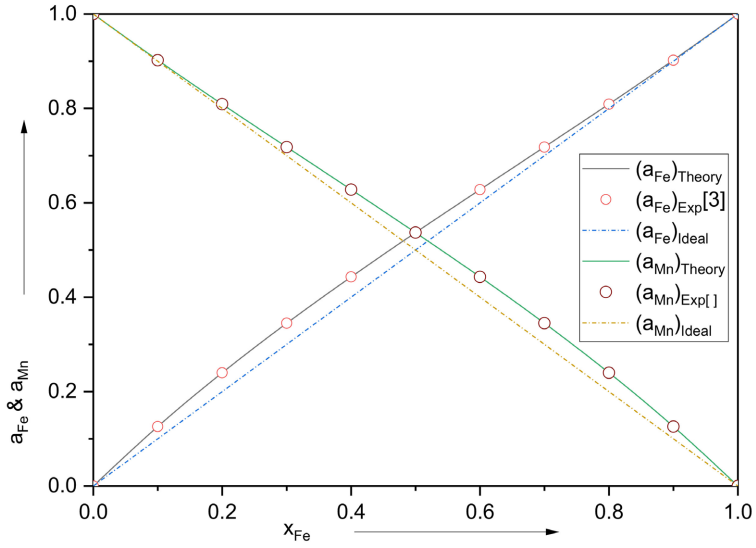


**Figure 4.** ( $a_{Fe}$ & $a_{Mn}$ ) vs $x_{Fe}$ for Fe-Mn melts at 1863 K.

A well harmony is noticed between theory and experiment [3]. The RMS error for $a_{Fe}$ and $a_{Mn}$ are 0.000252% and 0.000238% respectively. The positive deviations of $a_{Fe}$ and $a_{Mn}$ from ideal behaviour indicate the segregating nature of Fe-Mn melts at 1863 K. The agreement between theory and experimental data validates the estimated values of $A_{ji}$ and $A_{ij}$ .

### 3.2. Microscopic Properties *i.e.* $S_{cc}(0)$ and $\alpha_1$ of Fe-Mn Molten Melts at 1863 K

Expressions (14) and (15) are employed to compute the concentration dependence of $S_{cc}(0)$ for Fe-Mn melts at 1863 K. The theoretical data of $S_{cc}(0)$ are incorporated in **Figure 5** along with $S_{cc}^{id}(0)$ and experimental values [3].

A well uniformity is observed between the theory and experiment. The RMS error for $S_{cc}(0)$ is found to be 0.000124%. It is noticed that $S_{cc}(0) > S_{cc}^{id}(0)$ in the composition region, $x_{Fe} = 0.1$ to 0.9 and $S_{cc}(0)$ exhibits ideal behaviour of Fe-Mn melts at 1863 K in the region $0.0 \le x_{Fe} \le 0.1$ and $0.9 \le x_{Fe} \le 1.0$ . The similar behaviour of Fe-Mn melts is observed in the region $0.0 \le x_{Fe} \le 0.2$ and $0.9 \le x_{Fe} \le 1.0$ [13]. Thus, the present theoretical investigation confirms the segregating character of Fe-Mn melt at 1863 K. The maximum values of $S_{cc}(0)$ are at $x_{Fe} = 0.50$ *i.e.* $S_{cc}(0)\left(\max^{m}\right) = 0.293$ (Theory) and 0.291 (Experiment).

The theoretical values of $S_{cc}(0)$ for Fe-Mn melts at 1863 K available in the literature [13] exhibit some discrepancies with the experimental data in the region $0.2 \le x_{Fe} \le 0.5$. This indicates that the present theoretical model provides comparatively better results in comparison to the data available in the literature [13].

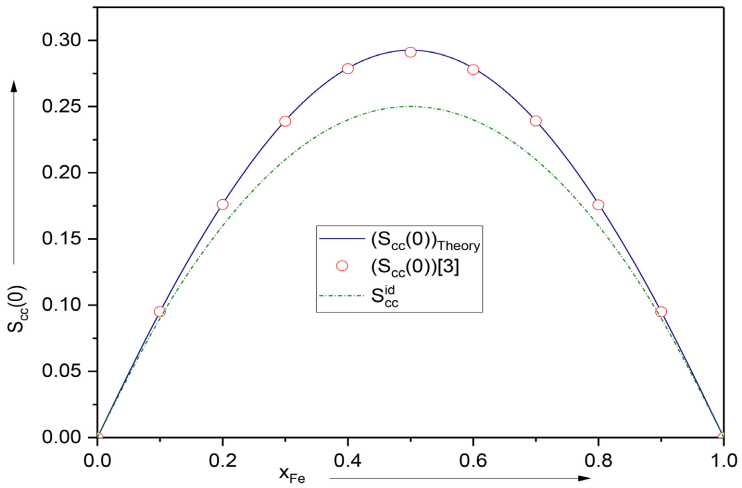


**Figure 5.** $S_{cc}(0)$ vs $x_{Fe}$ for Fe-Mn melts at 1863 K.

Equation (18) is used to achieve the concentration dependent values of $\alpha_1$ for Fe-Mn melts at 1863 K on using $Z = 10$. The theoretical data of $\alpha_1$ in terms of the concentration of Fe are presented in **Figure 6**. In the whole of composition *i.e.* $x_{Fe} = 0.1$ to 0.9, $\alpha_1$ is positive at each composition and having maximum value of 0.0148 at $x_{Fe} = 0.5$, which confirms the segregation in Fe-Mn melts at 1863 K. It is necessary to state that the present theoretical investigation suggests the symmetric behaviour of Fe-Mn melts at 1863 K which differs with the theoretical data of $\alpha_1$ suggested by Ogundenji *et al.* [13] on using self-association model.

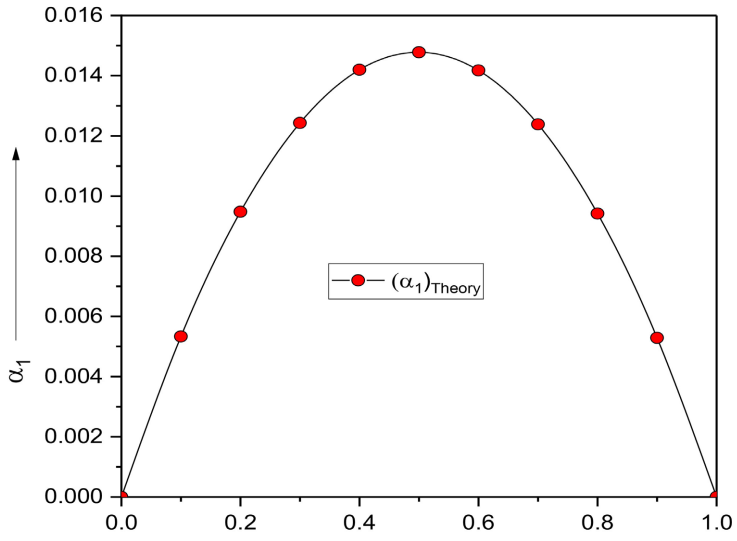


**Figure 6.** $\alpha_1$ vs $x_{Fe}$ for Fe-Mn melts at 1863 K.

### 3.3. $G_M^E$, $G_M$, $a_{Fe}$, $a_{Mn}$, $S_{cc}(0)$, $E^{XS}$, $\alpha_1$ and $D_M/D_{id}$ of Fe-Mn Melts at Different Temperatures

The concentration and temperature dependence of $G_M$, $S_{cc}(0)$, $\alpha_1$ and $D_M/D_{id}$ for Fe-Mn melts have been analysed by MIVM model. The necessary input parameters determined at 1763 K, 1863 K 1963 K and 2063 K are presented in Table 1 and Table 2. The values of pair potential parameters $A_{ji}$ and $A_{ij}$ are determined at 1763 K, 1863 K, 1963 K and 2063 K on using the following equations [16]

$$-\frac{\varepsilon_{ji}-\varepsilon_{ii}}{kT}=T\ln A_{ji}(T)=T_0\ln A_{ji}(T_0)$$

$$A_{ji}(T)=\exp\left(\frac{T_0\ln A_{ji}(T_0)}{T}\right) \tag{22}$$

and

$$-\frac{\varepsilon_{ij}-\varepsilon_{jj}}{kT}=T\ln A_{ij}(T)=T_0\ln A_{ij}(T_0)$$

$$A_{ij}=\exp\left(\frac{T_0\ln A_{ij}(T_0)}{T}\right) \tag{23}$$

where, $T_0$ = 1863 K and $T$K = required temperatures.

The values of $A_{ji}$ and $A_{ij}$ determined at different temperature, are included in Table 2.

Now, Equation (1) is utilised to determine the concentration dependence of $G_M^E/RT$ at 1763 K, 1863 K, 1963 K and 2063 K for Fe-Mn melts. The theoretical data of $G_M^E/RT$ as a function of composition of Fe are illustrated in Figure 7. The theoretical and experimental data of $G_M^E/RT$ for Fe-Mn melts at 1863 K are also presented in Figure 7. It is found that the values of $G_M^E/RT$ decline on raising the temperature from 1763 K to 2063 K. However, the position of maxima remains same *i.e.* at $x_{Fe}=0.50$ *i.e.* $G_M^E/RT\left(\max^{m}\right)=0.0763$, 0.0710, 0.0657 and 0.0614 at 1763 K, 1863 K, 1963 K and 2063 K respectively. This signifies the degradation of the segregating behaviour of Fe-Mn melts when the temperature rises from 1763 K to 2063 K.

Equations (1) and (13) are utilized to compute $G_M/RT$ at 1763 K, 1963 K and 2063 K for Fe-Mn melts. The theoretical data of $G_M/RT$ for Fe-Mn melts at 1863 K are shown in Figure 8 along with the theoretical and experimental data [3]. Obviously, the negative value of $G_M/RT$ increases with the increase in temperature from 1763 K to 2063 K, Nevertheless, the change in $G_M/RT$ is small in comparison to the rise in temperature and the position of minima remains same *i.e.* $x_{Fe}=0.50$. The values of $G_M/RT$ are minimum *i.e.* −0.6169, −0.6221, −0.6274 and −0.6317 respectively at 1763 K, 1863 K 1963 K and 2063 K. This shows the declination in the segregating behaviour of Fe-Mn melts with the rise in temperature.

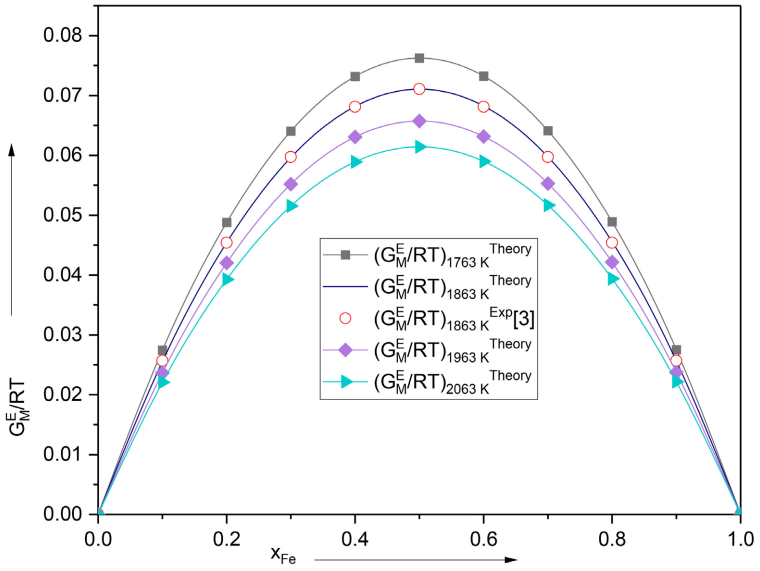


**Figure 7.** $G_M^E/RT$ vs $x_{Fe}$ for Fe-Mn melts at 1763 K, 1863 K, 1963 K and 2063 K.

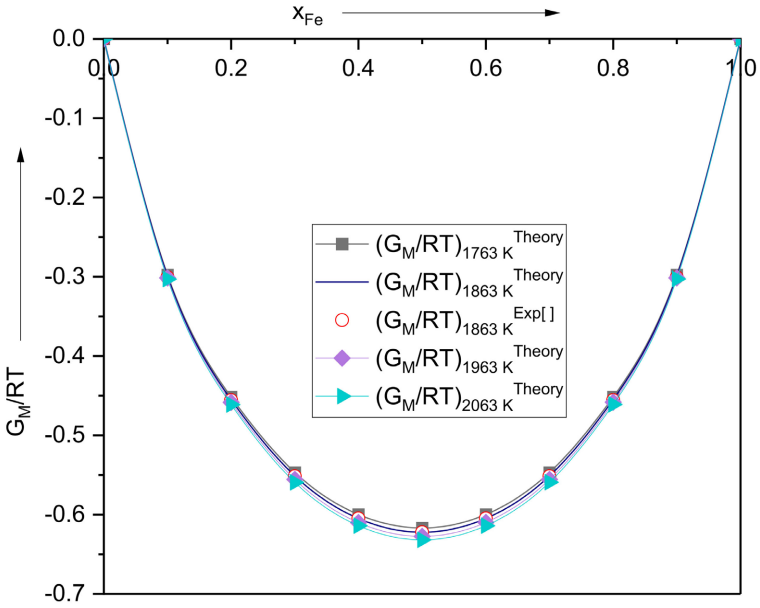


**Figure 8.** $G_M/RT$ vs $x_{Fe}$ for Fe-Mn melts at 1763 K, 1863 K, 1963 K and 2063 K.

The concentration and temperature dependency of Fe-Mn melts have been analysed in terms of $a_{Fe}$ and $a_{Mn}$. The Equations (10a) and (10b) are employed to compute $a_{Fe}$ and $a_{Mn}$ as a function of the composition of Fe at 1763 K, 1963 K and 2063 K. The theoretical data of $a_{Fe}$ and $a_{Mn}$ at 1763 K, 1863 K, 1963 K and 2063 K are depicted in **Figure 9**. Obviously, $a_{Fe}$ and $a_{Mn}$ exhibit positive deviations from linear law at each temperature under consideration. However, the deviations of $a_{Fe}$ and $a_{Mn}$ from linearity are found to be slightly decreased with the rise in temperature from 1763 - 2063 K. This indicates the lowering of the segregation in Fe-Mn melts due to rise in temperature from 1763 K to 2063 K.

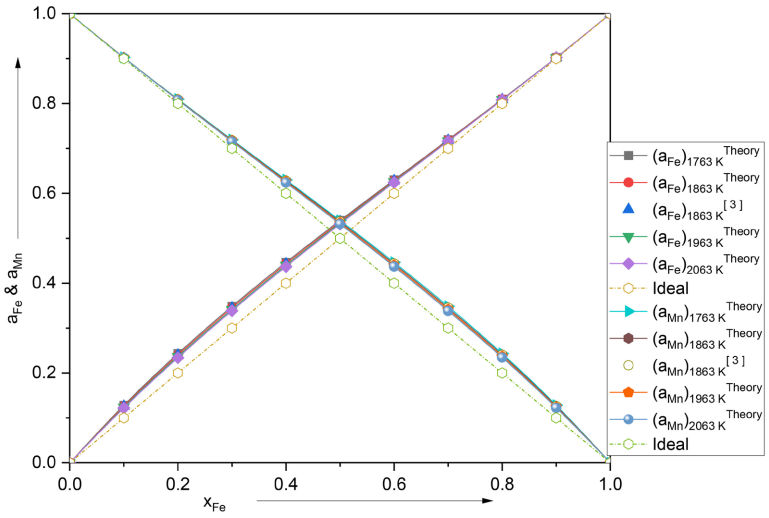


**Figure 9.** ( $a_{Fe}$ & $a_{Mn}$ ) vs $x_{Fe}$ for Fe-Mn melts at 1763 K, 1863 K, 1963 K and 2063 K.

The theoretical values of $S_{cc}(0)$ for Fe-Mn melts at 1763 K, 1963 K and 2063 K are ascertained from Equations (14) and (15) which are depicted in **Figure 10** along with $S_{cc}^{id}(0)$. For comparison, the experimental values of $S_{cc}(0)$ at 1863 K are also included in **Figure 10**. It is clear that $S_{cc}(0) > S_{cc}^{id}(0)$ at each composition in full concentration range *i.e.* $x_{Fe} = 0.10$ to 0.90 at each temperature under consideration. However, the values of $S_{cc}(0)$ decrease due to elevation of temperature from 1763 K to 2063 K. This illustrates the decreasing behaviour of segregation in Fe-Mn alloys in the temperature range, 1763 - 2063 K. Further the symmetry in $S_{cc}(0)$ is maintained in the temperature region 1763 - 2063 K because the $S_{cc}(0)$ is maximum at $x_{Fe} = 0.50$ *i.e.* 0.295, 0.293, 0.288 and 0.286 at 1763 K, 1863 K 1963 and 2063 K.

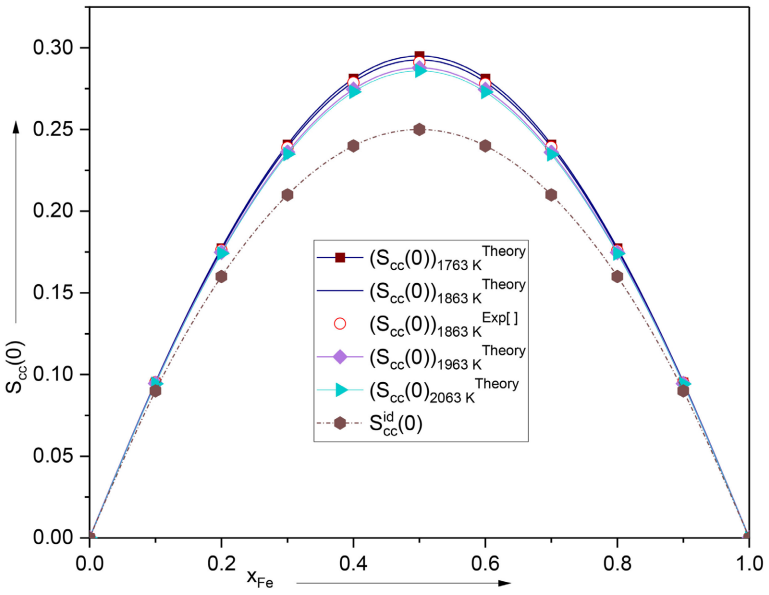


**Figure 10.** $S_{cc}(0)$ vs $x_{Fe}$ for Fe-Mn melts at 1763 K, 1863 K, 1963 K and 2063 K.

The concentration dependence of the excess stability function, $E^{XS}/RT$ for Fe-Mn alloys at 1763 K, 1863 K 1963 and 2063 K determined from Equation (19) are illustrated in **Figure 11**. Obviously, $E^{XS}/RT$ is negative at each composition of Fe in the concentration region $x_{Fe}=0.10$ to 0.90 at each temperature under consideration. Nevertheless, the negative magnitude of $E^{XS}/RT$ degrades due to rise in temperature from 1763 K to 2063 K. This is a sign of decrease in the segregation of Fe-Mn melts from 1763 K to 2063 K.

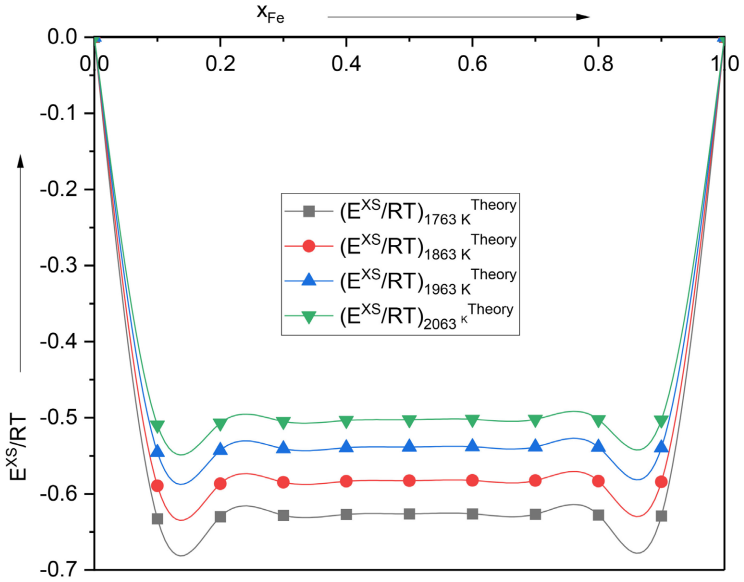


**Figure 11.** $E^{XS}/RT$ vs $x_{Fe}$ for Fe-Mn melts at 1763 K, 1863 K, 1963 K and 2063 K.

**Figure 12** exhibits the concertation and temperature dependence of $\alpha_1$ for Fe-Mn melts determined from Equation (18). At each concentration, $\alpha_1$ is positive at each temperature under consideration and its magnitude decreases with the rise in temperature in the region 1763 - 2063 K which shows the lowering in segregation of Fe-Mn alloys in the temperature range 1763 K to 2063 K. Again, the magnitude of $\alpha_1$ is small which illustrates that Fe-Mn melts are a weakly segregating system in the temperature range 1763 - 2063 K.

The diffusivity ratio, $D_M/D_{id}$ as a function of the composition of Fe for Fe-Mn melts at 1763 K, 1863 K, 1963 K and 2063 K are calculated from Equation (20) and the theoretical values of $D_M/D_{id}$ are depicted in **Figure 13**. It is noticed that diffusivity ratio, $D_M/D_{id}<1$ in the region $0.1\le x_{Fe}\le 0.9$ and has minimum values of 0.8434, 0.8543, 0.8654 and 0.8744 respectively at 1763 K, 1863 K, 1963 K and 2063 K around the equiatomic composition, $x_{Fe}=0.5$ for Fe-Mn melts. Again, due to rise in temperature from 1763 K to 2063 K, the values of $D_M/D_{id}$ increase at each concentration which is a sign of degradation in the segregating behaviour of Fe-Mn melts due to elevation of temperature from 1763 K to 2063 K. Therefore, the present theoretical investigation suggests that the probability of phase separation is maximum at $x_{Fe}=0.5$ which is also suggested by Ogundenji *et al.* [13].

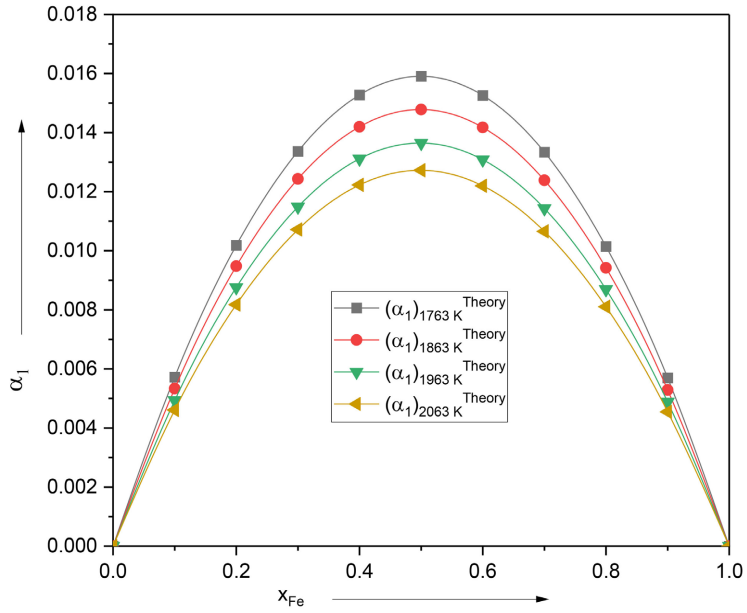


**Figure 12.** $\alpha_1$ vs $x_{Fe}$ for Fe-Mn melts at 1763 K, 1863 K, 1963 K and 2063 K.

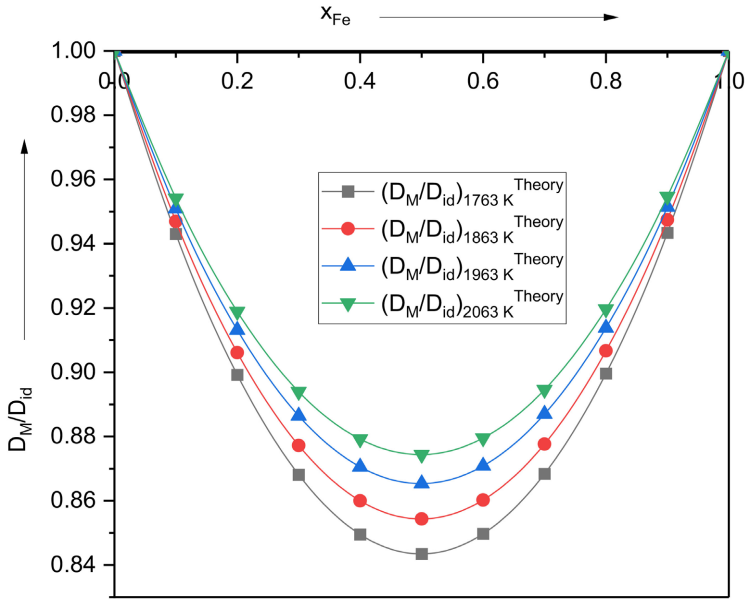


**Figure 13.** $D_M/D_{id}$ vs $x_{Fe}$ for Fe-Mn melts at 1763 K, 1863 K, 1963 K and 2063 K.

## 4. Conclusion

The present theoretical study successfully explores the mixing behaviour of Fe-Mn melts in terms of the composition of Fe at 1763 K, 1863 K, 1963 K and 2063 K in which the results for $G_M^E$, $G_M$, $\gamma_{Fe}$, $\gamma_{Mn}$, $a_{Fe}$, $a_{Mn}$ and $S_{cc}(0)$ at 1863 K are validated from experimental results while the results for $\alpha_1$, $E^{XS}$ and $D_M/D_{id}$ at 1863 K are the theoretical predictions for Fe-Mn melts. Again, the results for the aforesaid properties of Fe-Mn melts at 1763, 1963 and 2063 K are model predictions extrapolated from the results at 1863 K. Therefore, the

results suggest that Fe-Mn melt is a feebly segregating system in the temperature region 1763 - 2063 K, *i.e.* similar atoms (Fe-Fe or Mn-Mn) associate together as the closest neighbour. Further, the concentration and temperature reliance of the properties like $G_M^E$, $G_M$, $S_{cc}(0)$, $\alpha_1$, $E^{XS}$ and $D_M/D_{id}$ exhibits the symmetric behaviour of Fe-Mn melts about equiatomic composition, $x_{Fe}=0.5$ in the temperature region 1763 - 2063 K. Thus MIVM model is found to be a reliable model.

## Author Contributions

Conceptualization, I. S. Jha and J. Mandal; methodology, N. K. Roy; validation, I. S. Jha, J. Mandal and N. Vrind; formal analysis, R. Prabhu; investigation, S. K. Bhagat; writing original draft preparation, N. Vrind; writing-review and editing, N. K. Roy; visualization, I. S. Jha; supervision, J. Mandal. All authors have read and agreed to published version of the manuscript.

## Conflicts of Interest

The authors declare no conflicts of interest regarding the publication of this paper.

## References

[1] Jacob, K.T., Hajra, J.P. and Iwase, M. (1984) Activities of Mn in Solid and Liquid Fe-Mn Alloys. *Archiv für das Eisenhüttenwesen*, **55**, 421-426. https://doi.org/10.1002/srin.198405368

[2] Chikova, O.A., Sinitsin, N.I. and V'yukhin, V.V. (2021) Electrical Resistivity of Liquid Fe-Mn Alloys. *Russian Physics Journal*, **64**, 1039-1046. https://doi.org/10.1007/s11182-021-02426-y

[3] Hultgren, R., Desai, P.D., Hawkins, D.T., Gleiser, M. and Kelley, K.K. (1973) Selected Values of the Thermodynamic Properties of Binary Alloys. ASM.

[4] Lee, J., Thu Hoai, L. and Shin, M. (2011) Density and Surface Tension of Liquid Fe-Mn Alloys. *Metallurgical and Materials Transactions B*, **42**, 546-549. https://doi.org/10.1007/s11663-011-9490-9

[5] Thu Hoai, L. and Lee, J. (2011) Density of Liquid Fe-Mn-C Alloys. *Metallurgical and Materials Transactions B*, **42**, 925-927. https://doi.org/10.1007/s11663-011-9555-9

[6] Chen, H., Gao, L., Zhan, W., He, Z. and Zhang, J. (2022) Application of the Molecular Interaction Volume Model for Calculating Activities of Elements in Ferromanganese Alloys: Mn-C, Mn-Fe, Fe-C, and Mn-Fe-C Systems. *Crystals*, **12**, Article 682. https://doi.org/10.3390/cryst12050682

[7] Huang, W. (1989) An Assessment of the Fe-Mn System. *Calphad*, **13**, 243-252. https://doi.org/10.1016/0364-5916(89)90004-7

[8] Witusiewicz, V.T., Sommer, F. and Mittemeijer, E.J. (2003) Enthalpy of Formation and Heat Capacity of Fe-Mn Alloys. *Metallurgical and Materials Transactions B*, **34**, 209-223. https://doi.org/10.1007/s11663-003-0008-y

[9] Paek, M., Jeon, J. and Lindberg, D. (2020) Thermodynamic Behaviour of Nitrogen in the Carbon Saturated Fe-Mn-Si Alloy during Casting. *International Journal of Cast Metals Research*, **33**, 226-232. https://doi.org/10.1080/13640461.2020.1834176

[10] Raman, S., Hoyt, J.J., Saidi, P. and Asta, M. (2020) Molecular Dynamics Study of the

Thermodynamic and Kinetic Properties of the Solid-Liquid Interface in FeMn. *Computational Materials Science*, **182**, Article ID: 109773. https://doi.org/10.1016/j.commatsci.2020.109773

[11] Lintzen, S., von Appen, J., Hallstedt, B. and Dronskowski, R. (2013) The Fe-Mn Enthalpy Phase Diagram from First Principles. *Journal of Alloys and Compounds*, **577**, 370-375. https://doi.org/10.1016/j.jallcom.2013.06.006

[12] Bao, S., Tangstad, M., Tang, K., Einarsrud, K.E., Syvertsen, M., Onsøien, M., *et al.* (2021) Investigation of Two Immiscible Liquids Wetting at Elevated Temperature: Interaction between Liquid FeMn Alloy and Liquid Slag. *Metallurgical and Materials Transactions B*, **52**, 2847-2858. https://doi.org/10.1007/s11663-021-02222-6

[13] Ogundeji, S.O., Awe, O.E., Madu, C.A. and Anusionwu, B.C. (2021) Fe-Co and Fe-Mn Liquid Alloys: A Study of Bulk and Transport Properties. *Journal of Molecular Liquids*, **328**, Article ID: 115393. https://doi.org/10.1016/j.molliq.2021.115393

[14] Warren, B.E. (1969) X-Ray Diffraction. Addition-Weseley.

[15] Cowley, J.M. (1950) An Approximate Theory of Order in Alloys. *Physical Review*, **77**, 669-675. https://doi.org/10.1103/physrev.77.669

[16] Tao, D.P. (2000) A New Model of Thermodynamics of Liquid Mixtures and Its Application to Liquid Alloys. *Thermochimica Acta*, **363**, 105-113. https://doi.org/10.1016/s0040-6031(00)00603-1

[17] Ding, G.H., Liang, L.M., Meng, P., Wang, L., Wang, Y.X., Wang, Y.J., *et al.* (2020) Application of the Molecular Interaction Volume Model to the Assessment of Thermodynamic Properties of Liquid Zn-Bi Alloys. *Metallic Materials*, **57**, 55-60. https://doi.org/10.4149/km_2019_1_55

[18] Watanabe, M., Adachi, M. and Fukuyama, H. (2022) Densities of Au-X (X = Cu, Ni and Pd) Binary Melts and Thermodynamic Correlations. *Journal of Molecular Liquids*, **348**, Article ID: 118050. https://doi.org/10.1016/j.molliq.2021.118050

[19] Odusote, Y.A., Jabar, J.M., Bolarinwa, H.S. and Akinbisehin, A.B. (2019) Application of Molecular Interaction Volume Model in Separation of Ti-Al Alloys in Vacuum Distillation. *Vacuum*, **169**, Article ID: 108885. https://doi.org/10.1016/j.vacuum.2019.108885

[20] Liang, L.M., Ding, G.H., Wang, Y.X. and Liu, Y. (2020) Thermodynamic Properties of Liquid Zn-Cd Alloys Investigated by the Molecular Interaction Volume Model. *Physics and Chemistry of Liquids*, **59**, 706-715. https://doi.org/10.1080/00319104.2020.1808655

[21] Sah, S.K., Jha, I.S. and Koirala, I. (2023) Theoretical Examination of Some Thermodynamic Properties in In-Bi-Sn Liquid Alloy and Its Sub-Binary Systems. *Journal of Electronic Materials*, **52**, 6350-6359. https://doi.org/10.1007/s11664-023-10571-y

[22] Odusote, Y.A., Popoola, A.I., Adedayo, K.D. and Ogunjo, S.T. (2017) Thermodynamic Properties of Al in Ternary Lead-Free Solder Al-Sn-Zn Alloys. *Materials Science-Poland*, **35**, 583-593. https://doi.org/10.1515/msp-2017-0080

[23] Sah, S.K., Jha, I.S. and Koirala, I. (2024) Thermodynamic Activity in Zn-Cu-Sn-In Liquid Solder Alloys: A Comprehensive Analysis Using the Molecular Interaction Volume Model. *Welding International*, **38**, 265-276. https://doi.org/10.1080/09507116.2024.2325151

[24] You, Y., Kong, L., Xu, J., Xu, B., Liu, G. and Yang, B. (2021) Prediction of Activities of All Components in Sn-Ag-Cu and Sn-Ag-Cu-Zn Lead-Free Solders Using Modified Molecular Interaction Volume Model. *Results in Chemistry*, **3**, Article ID: 100143. https://doi.org/10.1016/j.rechem.2021.100143

[25] Singh, R.N. and Sommer, F. (1997) Segregation and Immiscibility in Liquid Binary Alloys. *Reports on Progress in Physics*, **60**, 57-150. https://doi.org/10.1088/0034-4885/60/1/003

[26] Bhatia, A.B. and Thornton, D.E. (1970) Structural Aspects of the Electrical Resistivity of Binary Alloys. *Physical Review B*, **2**, 3004-3012. https://doi.org/10.1103/physrevb.2.3004

[27] Bhatia, A.B. and Hargrove, W.H. (1974) Concentration Fluctuations and Thermodynamic Properties of Some Compound Forming Binary Molten Systems. *Physical Review B*, **10**, 3186-3196. https://doi.org/10.1103/physrevb.10.3186

[28] Singh, R.N. (1987) Short-Range Order and Concentration Fluctuations in Binary Molten Alloys. *Canadian Journal of Physics*, **65**, 309-325. https://doi.org/10.1139/p87-038

[29] Darken, L.S. (1967) Thermodynamics of Binary Metallic Solutions. *Transactions of the Metallurgical Society of AIME*, **239**, 80.

[30] Singh, A.P., Chaudhary, R.P., Kumari, R., Jha, I.S. and Mandal, J. (2022) Stability of Nak Liquid Alloys at Different Temperatures. *Materials Today*: *Proceedings*, **66**, 2251-2258. https://doi.org/10.1016/j.matpr.2022.06.097

[31] Darken, L.S. and Aime, M.L. (2010) Diffusion, Mobility and Their Interrelation through Free Energy in Binary Metallic Systems. *Transactions of the AIME*, **175**, 184-201.

[32] Iida, T. and Guthrie, R.I.L. (1988) The Physical Properties of Liquid Metals. Clarendon Press.